Letter

Electronic correlations and topology in Kondo insulator PuB_6

K. Gofryk,[1,2,*] S. Zhou,[2] N. Poudel,[3] N. Dice,[3] D. Murray,[3] T. Pavlov,[3] and C. Marianetti[4]
[1]*Center for Quantum Actinide Science and Technology, Idaho National Laboratory, Idaho Falls, Idaho 83415, USA*
[2]*Glenn T. Seaborg Institute, Idaho National Laboratory, Idaho Falls, Idaho 83415, USA*
[3]*Idaho National Laboratory, Idaho Falls, Idaho 83415, USA*
[4]*Department of Applied Physics and Applied Mathematics, Columbia University, New York, New York 10027, USA*

(Received 5 March 2025; accepted 14 November 2025; published 5 January 2026)

Utilizing a combination of dynamical mean field theory (DMFT) and density functional theory, it has been theoretically proposed that PuB_6 is a strongly correlated topological insulator characterized by nontrivial $\mathbf{Z}_2$ topological invariants and metallic surface states [X. Deng *et al.*, Phys. Rev. Lett. **111**, 176404 (2013)]. Here, we demonstrate through low-temperature magnetotransport measurements and first-principles calculations that PuB_6 exhibits characteristics of a topological Kondo insulating state. These features include a transition in electrical resistivity from high-temperature, thermally activated behavior with a narrow gap at the Fermi level ($\Delta\rho \sim 20$ meV) to a distinctive low-temperature plateau, as well as a surface-to-volume dependence of electrical resistivity at low temperatures. The topological nature of PuB_6 is further supported by the theoretical calculations, which show that GGA + U is capable of capturing electronic, topological, and lattice properties of PuB_6 with much lower computational cost than DMFT.

DOI: 10.1103/hwpn-gll9

Introduction. The concept of strongly correlated topological insulators is highly appealing not only because the surface states, protected from backscattering by time-reversal symmetry, may host massless charge carriers with locked helical spin polarization, but also because the surface of such correlated system may exhibit nontrivial electronic structures not present in conventional band insulators (for a review, see, e.g., Refs. [1,2]). The $5f$-electron materials, in particular, possess all the essential ingredients for hosting topological phenomena. These include strong spin-orbit coupling (SOC), electrons of opposite parity (e.g., $5f$ versus $5d$) that are inverted in energy in particular sections in the Brillouin zone, and a large f-f overlap, which results in larger energy scales. Since most relevant electronic interactions have similar energy scales, combining strong electronic interactions and topology offers a unique way to control topological properties. To date, only a handful of $5f$-electron-based systems have been predicted or demonstrated to host topological phenomena, which include a family of topological Mott insulators, AnX, where An = Pu, Am and X = pnictogen and chalcogen elements [3], $U_3Bi_4Ni_3$ Kondo insulator [4], $UCo_{0.8}Ru_{0.2}Al$ ferromagnet (Weyl semimetal with large Nernst effect) [5], UTe_2 (Weyl superconductor) [6,7], UOTe antiferromagnet (Dirac semimetal) [8], and/or PuB_4 topological insulator [9,10].

Topological Kondo insulators, in particular, have garnered significant interest in the field of strongly correlated electronic systems, with special attention devoted to samarium hexaboride (SmB_6) [11], which has been proposed as the first member of this family [12–16]. This discovery has spurred huge scientific interests, both theoretically [15–19] and experimentally [20–26], although several inconsistencies remain regarding the specifics of its topological nature. Similar CeB_6 and YbB_6 have also been predicted to exhibit nontrivial electronic structure [27,28], but experimental studies have not supported these predictions [29,30]. Recently, it has been proposed theoretically that PuB_6 is an intermediate-valent, strong topological insulator with nontrivial $\mathbf{Z}_2$ topological invariants [31]. Its surface states are predicted to contain three Dirac cones with a large Fermi pocket at the X point, a characteristic feature of cubic topological Kondo insulators [19]. However, experimental validation of the electronic ground state and its relationship to the topological characteristics in PuB_6 remain lacking.

In this Letter, we address this topic by investigating the low-temperature electronic properties of PuB_6 through synthesis and micromachining characterization, magnetotransport measurements, and detailed electronic structure calculations. The electrical resistivity reveals a narrow energy gap at the Fermi level and can be described by a two-conductivity channel model that accounts for both metallic and semiconducting components, similar to other topological insulators. The presence of surface states is further supported by the low-temperature resistivity plateau and the dependence of electrical resistivity on crystal geometry (surface-to-volume ratio). The magnetoresistivity measurements indicate incomplete surface dominance of the interplay between Dirac and conventional carriers rather than a single

*Contact author: gofryk@inl.gov

pristine topological transport channel in PuB_6. This work demonstrates that PuB_6 is a compelling candidate for investigating the influence of electronic correlations and topology, supporting theoretical predictions of an insulating bulk with metallic surface states. We discuss the implications of this study and the role of increased f-f overlap and the resulting energy scales on the topological characteristics when transitioning from widely studied $4f$-electron systems to actinide-based topological materials.

Methods. Polycrystalline samples of PuB_6 were synthesized by a standard arc melting technique. In PuB_6, this synthesis method can lead to a multiphase sample that contains a mixture of cubic PuB_6 and tetragonal PuB_4 [32,33], rendering it unsuitable for bulk measurements. To overcome these issues, we utilized an FEI Helios plasma focus ion beam (PFIB) microscope to characterize, extract, and prepare microsized crystals of PuB_6 that are suitable for low-temperature magnetotransport measurements (see also Ref. [34]). The FIB micromachining approach was proven revolutionary for studying the magnetotransport properties of various p, d, f-electron topological materials [34–36] and very recently uranium systems [37,38]. The polycrystalline sample was first examined in the PFIB microscope using backscattered electron imaging, energy dispersive spectroscopy, and electron backscattered diffraction to locate a single crystal grain of interest and verify its crystallographic structure and grain orientation (see Fig. 1). Our polycrystalline button was a mixture of PuB_6 and PuB_4, and the structural analysis confirmed that the expected cubic ($Pm3m$) and tetragonal ($P4/mbm$) crystal structures can be identified with lattice parameters: $a = 4.129(3)$ Å, and $a = b = 7.313(8)$ Å and $c = 4.098(9)$ Å, respectively (see Fig. 1). These values are very close to the ones previously reported for these phases [32,39–41]. It is worth mentioning that due to the multiphase nature of the samples obtained we were unable to perform any bulk measurements such as heat capacity, magnetization, and especially angle-resolved photoemission spectroscopy to directly probe electronic structure in PuB_6. Once a suitable grain of PuB_6 phase was located, extracted, and structurally characterized (crystallographic orientation), it was transferred to a sapphire chip with contacts patterned by photolithography. Electrical contacts (platinum in our case) were then deposited onto the crystal with ion-assisted chemical vapor deposition [34,42]. Further details regarding the preparation and quantity of electrical contacts can be found in Ref. [33]. Low-temperature magnetotransport measurements were performed using a Quantum Design DynaCool-9 system and a standard four-point method. Density functional theory (DFT) calculations were carried out using the projector augmented-wave method [43,44], as implemented in the Vienna *Ab Initio* Simulation Package (VASP) [45,46]. The generalized gradient approximation (GGA) as formulated by Perdew, Burke, and Ernzerhof [47] was employed with a plane-wave cutoff energy of 600 eV. The $14 \times 14 \times 14$ Γ-centered k-point mesh and an energy convergence criterion of 10^{-6} eV were applied for the primitive cell. DFT + U was applied on Pu $5f$ electrons by using the simplified rotationally invariant approach [48,49]. All symmetry was turned off, and spin-orbit coupling was applied except when explicitly mentioned. Furthermore, the occupation matrix control approach was used to address the issue of many metastable electronic states in DFT + U [50], while more details can be found in the Supplemental Material [51]. Finally, to match with the nonmagnetic (NM) semiconducting nature of PuB_6 from dynamical mean field theory (DMFT) calculations [31] and experiments, we employed DFT calculations in NM order. However, please note that by using GGA + U for PuB_6, magnetic orderings are predicted to have lower energy than NM ordering, while having a metallic nature (see the Supplemental Material [51]). This is due to the limitations of DFT + U, where it predominantly captures singlet states without symmetry breaking. Similar results have been reported in δ-Pu [52,53].

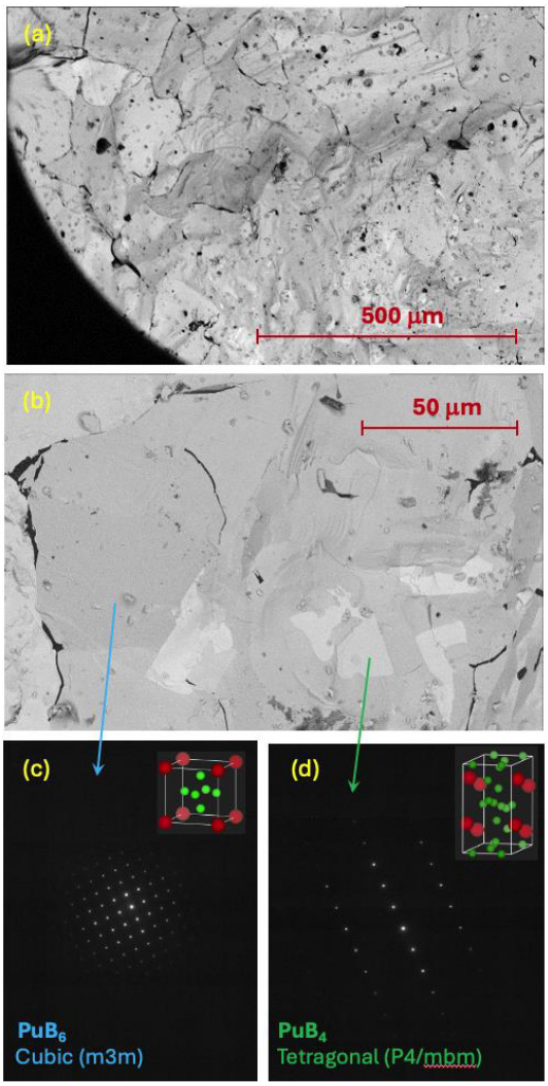

FIG. 1. (a), (b) Scanning electron microscope micrographs of arc-melted sample of PuB_6 showing a mixture of PuB_6 and PuB_4, as identified by selected area diffraction. (c), (d) The insets show the crystallographic structure of cubic ($m3m$) PuB_6 and tetragonal ($P4/mbm$) PuB_4 (see more details in the text).

Magnetotransport studies. Figure 2(a) displays the temperature dependence of the electrical resistivity of single-crystal lamellas of PuB_6, measured for crystals with different geometries and with the electrical current (i) applied along the ⟨100⟩ crystallographic direction (see the insets of Fig. 2).

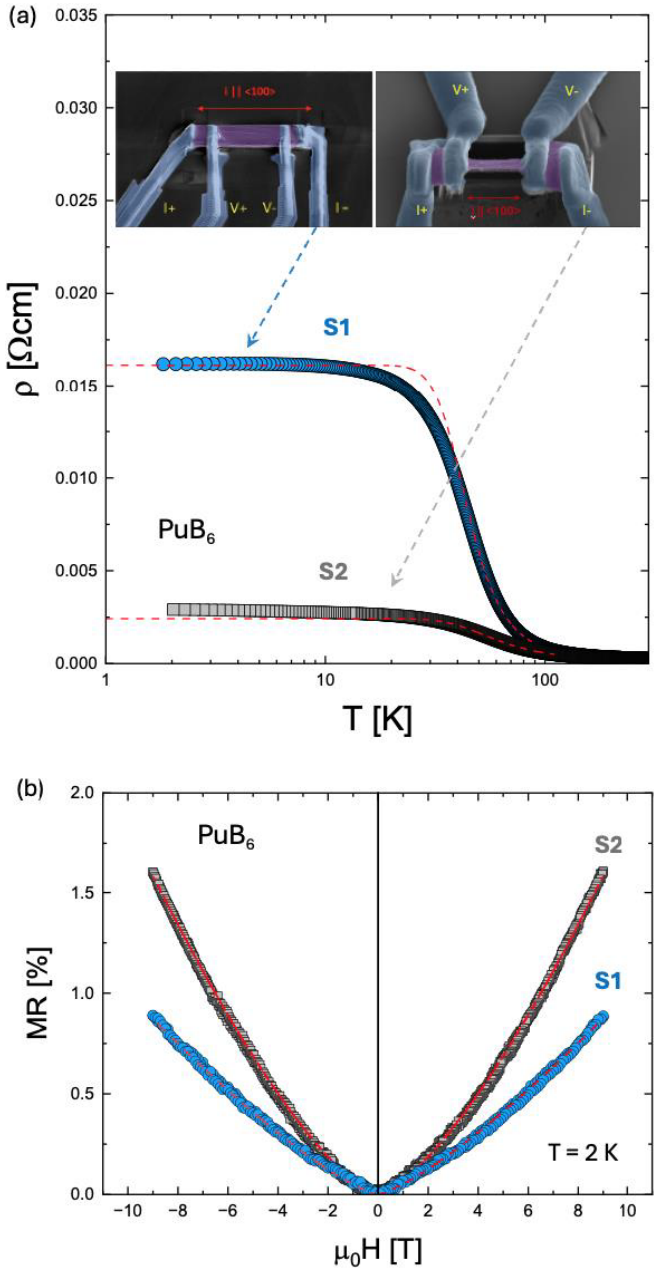

FIG. 2. (a) The temperature dependence of the electrical resistivity of the PuB_6 microcrystals. Samples' dimensions (thickness × width × length) are 3.4 μm × 6.7 μm × 31 μm and 0.5 μm × 1 μm × 20 μm, respectively, for samples S1 and S2. The dashed lines represent fits to the data using a two-channel conductance model (see the text). The insets show PFIB lamellas of PuB_6 prepared for low-temperature transport measurements ($i||\langle 100\rangle$). (b) The magnetic field dependence of transverse magnetoresistivity of PuB_6 crystals measured at $T = 2$ K. The dashed line represents the relation MR $\sim H^{1.3}$ for sample S1 and MR $\sim H^{1.4}$ for sample S2.

As shown, the $\rho(T)$ curves exhibit semiconductinglike behavior down to ∼30 K, below which a resistivity plateau is observed. In this regard, the overall $\rho(T)$ dependence resembles that observed in nonmagnetic topological insulators, where band inversion leads to the existence of the metallic surface modes protected by time-reversal symmetry [54–56]. The transition from high-temperature, thermally activated behavior to a low-temperature plateau in $\rho(T)$ is interpreted as a shift from bulk state-dominated conduction to surface state-dominated conduction. This scenario is also consistent with the surface-to-bulk ratio dependence of the resistivity. As shown in Fig. 2(a), the resistivity decreases with increasing surface-to-bulk ratio (S/V), with S/V values of 0.9 and 6 μm^{-1} for samples S1 and S2, respectively, as expected due to the reduction in overall bulk conductance. To account for both surface and bulk contributions to the resistivity of PuB_6 crystal, we analyzed the electrical resistivity data using a two-channel model [see the red dashed line in Fig. 2(a)], which has previously been used to describe $\rho(T)$ dependence of SmB_6 [56]. In this approach, the total electrical conductivity $\sigma(T) = \rho(T)^{-1}$ is given by the equation $\sigma_{\text{tot}}(T) = \sigma_s + \sigma_b e^{-\frac{\Delta_\rho}{k_B T}}$, where σ_s is the surface contribution to the electrical conductivity (independent of temperature), σ_b is the bulk contribution to the conductivity, Δ_ρ is the energy gap at the Fermi level, and k_B is the Boltzmann constant. The analysis yields $\Delta_\rho = 20$ and 18 meV, $\sigma_s = 62.1$ and 405.4 $\Omega\,m^{-1}$, and $\sigma_b = 13.9 \times 10^{-3}$ and 11.9×10^{-3} $\Omega\,m^{-1}$, for S1 and S2 samples, respectively. As expected for topological insulators, the obtained energy gap is similar for the two samples with different surface-to-volume ratios. However, the values for σ_s and σ_b show a clear contrast in their relationship with samples' surface-to-volume ratio. While σ_b parameter is relatively independent of the samples' S/V ratio, σ_s exhibits a clear dependence on the samples' geometry with σ_s being much larger for S2, in agreement to what is expected for topological insulators. Furthermore, the value of Δ_ρ is 5–6 times smaller than $\Delta_{\text{DFT}} \sim 100$–120 meV obtained by DFT calculations (see below). Interestingly, PuB_4 has also been predicted to host a topological insulating ground state with an energy gap of about 250 meV due to strong spin-orbit interactions [9,10]. The derived resistivity gap has been estimated to be 35 meV [9].

Figure 2(b) shows the magnetic field dependence of the transverse magnetoresistivity (MR) measured at 2 K. As can be seen, the MR(H) curves can be described by the forms MR $\propto H^{1.3}$ and $H^{1.4}$, respectively, for samples S1 and S2 [see red dashed lines in Fig. 2(b)]. The classical magnetoresistance in metals or doped semiconductors with a closed free-electron Fermi surface increases quadratically with increasing magnetic field H for $\mu_H < 1$ and saturates when $\mu_H > 1$ (μ is the zero-magnetic-field mobility). Magnetoresistivity in ideal topological insulators is often discussed in the context of linear field dependence (MR $\propto H$) at low temperatures, especially for surface states with Dirac-like dispersion in the quantum limit. Such behavior has previously been observed in surfaces of topological insulators $MnBi_2Te_4$ [57], Ru_2Sn_3 [58], Dirac semimetal Cd_3As_2 [59], and other 3D Dirac materials [60,61]. A weak antilocalization effects and the linear magnetoresistivity was observed in the orbital component of MR at $T \sim 50$–100 mK in SmB_6[62]. In topological insulators with both bulk and surface conduction, quadratic bulk MR from parabolic bands and linear MR from the Dirac-like surface states can combine as intermediate power-law dependence [63], as observed in PuB_6. Additionally, as can be seen in Fig. 2(b), sample S1 (with more bulk weight) exhibits

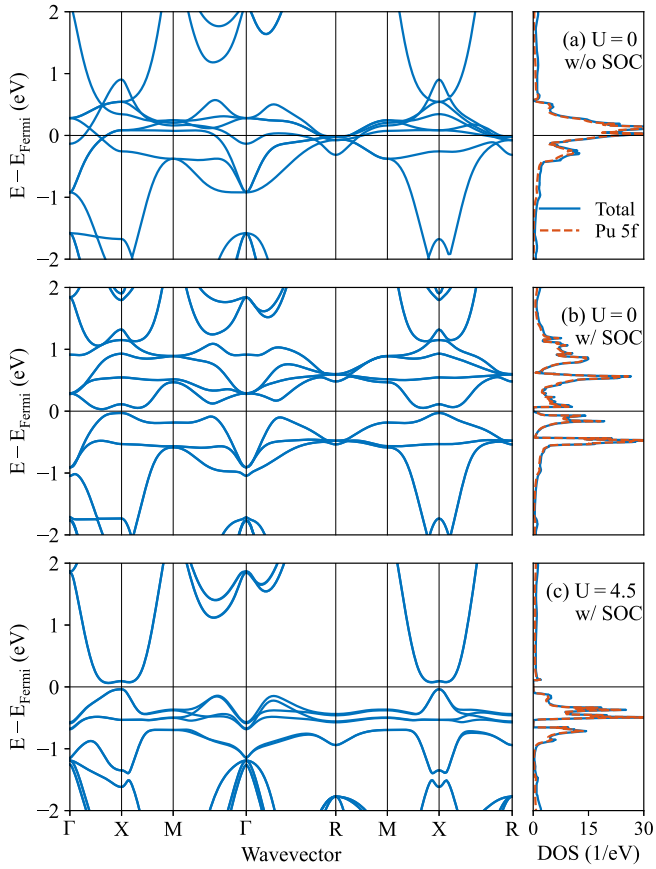

FIG. 3. Calculated electronic bands and DOS by using (a) GGA ($U = 0$ and without SOC), (b) GGA + SOC ($U = 0$), and (c) GGA + U + SOC ($U = 4.5$ eV). The solid blue curves represent total DOS, while dashed red curves present the partial DOS of Pu 5f electrons.

lower MR, while sample S2 (with more surface dominance) shows higher MR. Further magnetotransport experiments, particularly at very low temperatures, will be essential to draw definitive conclusions about the role of potential disorder, in-gap states, and/or localization effects in PuB_6.

DFT calculations. Here, DFT + U calculations are performed for PuB_6 as a static description of electron interactions at $T = 0$ K. Compared with DFT + DMFT, our DFT + U results show good agreements of predicted electronic properties with previous studies [31,64], while only taking a fraction of the computational cost. Therefore, DFT + U can be applied to study some complex properties, e.g., phonon properties, in PuB_6. The effect of SOC and the Hubbard U on the calculated electronic bands and density of states (DOS) is presented in Fig. 3. In GGA ($U = 0$ and without SOC), the Pu 5f electrons result in several nearly flat bands near the Fermi level E_{Fermi}, producing a metallic nature. By applying SOC, a band gap of 60.7 meV is opened. The band inversion produced by SOC, which is a signature of topological band insulator, can be observed in PuB_6 near the X point. Furthermore, by adding the Hubbard U, the Pu 5f states are further localized. Typically, the Hubbard U for Pu is in the range 4–4.5 eV [65–67]. For PuB_6, we used the linear response approach [68] to determine the Hubbard U, yielding $U = 3.74$ eV [see Ref. [69]], which

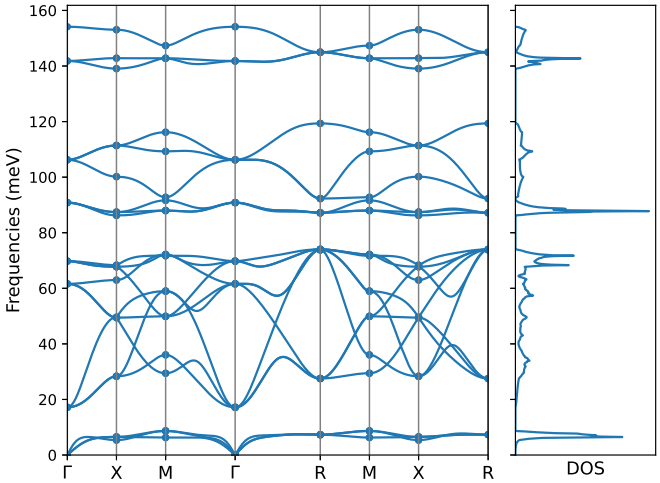

FIG. 4. Calculated phonon dispersion and DOS of PuB_6 by using GGA + U + SOC ($U = 4.5$ eV). The solid points were directly computed, while the corresponding lines are Fourier interpolations.

is reasonably close to the 4–4.5 eV range. While the Hubbard U value can quantitatively affect the value of lattice parameters and the band gaps, a band gap produced by band inversion is always observed for $U < 6.5$ eV (see the Supplemental Material [69]). Notably, our computed band structure shows great agreement with Ref. [31], for comparing both our GGA results [Fig. 3(b)] to their Local density approximation (LDA) results and our GGA + U [Fig. 3(c)] to their LDA + DMFT results, which uses the same $U = 4.5$ eV. We further developed a tight-binding model based on GGA + U + SOC calculation and computed the Z_2 topological invariant as well as electronic bands on (100) surface (see computational details and results in Ref. [69]). The computed Z_2 number is (1, 111), with a conducting surface band at $\bar{X}$ point, both of which are in good agreement with Ref. [31]. Additionally, we compute the phonon dispersion of PuB_6 by using GGA + U (see Fig. 4) and the lone irreducible derivative approach [70] with the $2 \times 2 \times 2$ supercell. While the absence of imaginary phonon frequencies confirms the structural stability in our calculation, and the phonon characteristics also indicate the d-f electron hybridization in PuB_6: similar to SmB_6 [71], phonon softening is observed for the two lowest optical branches near the Γ point and the longitudinal acoustic branch near the X point. Furthermore, phonon interaction calculations facilitated by DFT + U present opportunities to explore the insulating characteristics of PuB_6, for example, by isolating the contributions of electrons and phonons to thermal transport or illustrating the impact of vacancies, as observed in SmB_6 [72–74].

Summary and outlook. In summary, we performed synthesis, PFIB structural characterization and micromachining, and low-temperature magnetotransport measurements, along with detailed DFT calculations of PuB_6. We demonstrate that PFIB micromachining and characterization serve as excellent tools for investigating the magnetotransport properties of this 5f-electron quantum material. This is particularly crucial for transuranic materials, where conventional synthesis methods might lead to multiphase samples. Based on the results obtained, we provide experimental evidence that PuB_6

exhibits characteristics of topological Kondo insulating state, such as the presence of a narrow gap at the Fermi level ($\Delta_{\mathrm{DFT}} \sim 100\,\mathrm{meV}$ and $\Delta_\rho \sim 20\,\mathrm{meV}$), a characteristic low-temperature plateau of the electrical resistivity, the resistivity dependence on samples' surface-to-volume ratio, and MR dependence characteristic of topological insulators with both bulk and surface conduction. The intricate details of the nontrivial electronic structure of PuB_6 are further supported by theoretical calculations, where we show that GGA + U can accurately capture electronic, topological, and lattice properties of PuB_6 with much lower computational cost than DMFT. These results not only expand our understanding of this system beyond recent band structure calculations but also pave the way for a more profound comprehension between electronic correlations and topology in $5f$-electron materials.

Acknowledgments. The authors would like to thank Jason Jeffries and Mitchel Meyer for fruitful discussions. This work was supported by the U.S. Department of Energy, Basic Energy Sciences, Materials Sciences, and Engineering Division.

Data availability. The data that support the findings of this article are not publicly available. The data are available from the authors upon reasonable request.

[1] M. Z. Hasan and C. L. Kane, *Colloquium:* Topological insulators, Rev. Mod. Phys. **82**, 3045 (2010).
[2] N. P. Armitage, E. J. Mele, and A. Vishwanath, Weyl and Dirac semimetals in three-dimensional solids, Rev. Mod. Phys. **90**, 015001 (2018).
[3] X. Zhang, *et al.*, Actinide topological insulator materials with strong interaction, Science **335**, 1464 (2012).
[4] C. Broyles, *et al.*, High-temperature surface state in Kondo insulator $U_3Bi_4Ni_3$, Sci. Adv. **11**, eadq9952 (2025).
[5] T. Asaba, *et al.*, Colossal anomalous Nernst effect in a correlated noncentrosymmetric kagome ferromagnet, Sci. Adv. **7**, eabf1467 (2021).
[6] L. Jiao, *et al.*, Chiral superconductivity in heavy-fermion metal UTe_2, Nature (London) **579**, 523 (2020).
[7] T. Shishidou, *et al.*, Topological band and superconductivity in UTe_2, Phys. Rev. B **103**, 104504 (2021).
[8] C. Broyles, *et al.*, UOTe kondo-interacting topological antiferromagnet in a Van der Waals lattice, Adv. Mater. **37**, 2414966 (2025).
[9] H. Choi, *et al.*, Experimental and theoretical study of topology and electronic correlations in PuB_4, Phys. Rev. B **97**, 201114(R) (2018).
[10] D.-C. Ryu, *et al.*, Wallpaper Dirac fermion in a nonsymmorphic topological kondo insulator PuB_4, J. Am. Chem. Soc. **142**, 19278 (2020).
[11] A. Menth, E. Buehler, and T. H. Geballe, Magnetic and semiconducting properties of SmB_6, Phys. Rev. Lett. **22**, 295 (1969).
[12] Z. Fisk *et al.*, Kondo insulators, Physica B **206**, 798 (1995).
[13] H. Tsunetsugu, M. Sigrist, and K. Ueda, The ground-state phase diagram of the one-dimensional Kondo lattice model, Rev. Mod. Phys. **69**, 809 (1997).
[14] P. Riseborough, Heavy fermion semiconductors, Adv. Phys. **49**, 257 (2000).
[15] M. Dzero, K. Sun, V. Galitski, and P. Coleman, Topological kondo insulators, Phys. Rev. Lett. **104**, 106408 (2010).
[16] M. Dzero, J. Xia, V. Galitski, and P. Coleman, Topological kondo insulators, Annu. Rev. Condens. Matter Phys. **7**, 249 (2016).
[17] M. Dzero, K. Sun, P. Coleman, and V. Galitski, Theory of topological Kondo insulators, Phys. Rev. B **85**, 045130 (2012).
[18] F. Lu, J. Zhao, H. Weng, Z. Fang, and X. Dai, Correlated topological insulators with mixed valence, Phys. Rev. Lett. **110**, 096401 (2013).
[19] V. Alexandrov, M. Dzero, and P. Coleman, Cubic topological kondo insulators, Phys. Rev. Lett. **111**, 226403 (2013).
[20] H. Miyazaki, T. Hajiri, T. Ito, S. Kunii, and S.-i. Kimura, Momentum-dependent hybridization gap and dispersive in-gap state of the Kondo semiconductor SmB_6, Phys. Rev. B **86**, 075105 (2012).
[21] X. Zhang, *et al.*, Hybridization, inter-ion correlation, and surface states in the kondo insulator SmB_6, Phys. Rev. X **3**, 011011 (2013).
[22] D. J. Kim, *et al.*, Surface Hall effect and nonlocal transport in SmB_6 evidence for surface conduction, Sci. Rep. **3**, 3150 (2013).
[23] M. Neupane, *et al.*, Surface electronic structure of the topological Kondo-insulator candidate correlated electron system SmB_6, Nat. Commun. **4**, 2991 (2013).
[24] N. Xu, *et al.*, Surface and bulk electronic structure of the strongly correlated system SmB_6 and implications for a topological Kondo insulator, Phys. Rev. B **88**, 121102(R) (2013).
[25] J. Jiang, *et al.*, Observation of possible topological in-gap surface states in the Kondo insulator SmB_6 by photoemission, Nat. Commun. **4**, 3010 (2013).
[26] D. J. Kim, J. Xia, and Z. Fisk, Topological surface state in the Kondo insulator samarium hexaboride, Nat. Mater. **13**, 466 (2014).
[27] H. Weng, *et al.*, Topological crystalline kondo insulator in mixed valence ytterbium borides, Phys. Rev. Lett. **112**, 016403 (2014).
[28] R. Zhang, *et al.*, Weyl semimetal in the rare-earth hexaboride family supporting a pseudonodal surface and a giant anomalous Hall effect, Phys. Rev. B **105**, 165140 (2022).
[29] C.-J. Kang, *et al.*, Electronic structure of YbB_6: Is it a topological insulator or not? Phys. Rev. Lett. **116**, 116401 (2016).
[30] M. Neupane, *et al.*, Fermi surface topology and hot spot distribution in the Kondo lattice system CeB_6, Phys. Rev. B **92**, 104420 (2015).
[31] X. Deng, K. Haule, and G. Kotliar, Plutonium hexaboride is a correlated topological insulator, Phys. Rev. Lett. **111**, 176404 (2013).
[32] H. A. Eick, Plutonium borides, Inorg. Chem. **4**, 1237 (1965).
[33] See Supplemental Material at http://link.aps.org/supplemental/10.1103/hwpn-gll9 for Sec. VI: Synthesis and characterization, which provides a more detailed description of the synthesis process, as well as the preparation and evaluation of the electrical contacts.
[34] N. Poudel, *et al.*, Boundary scattering in topological Kondo insulator SmB_6, Appl. Phys. Lett. **126**, 192201 (2025).
[35] P. J. W. Moll, *et al.*, High magnetic-field scales and critical currents in SmFeAs(O, F) crystals, Nat. Mater. **9**, 628 (2010);

Evidence for hydrodynamic electron flow in $PdCoO_2$, Science **351**, 1061 (2016); Transport evidence for Fermi-arc-mediated chirality transfer in the Dirac semimetal Cd3As_2, Nature (London) **535**, 266 (2016).

[36] I. Antonyshyn, *et al.*, Micro-scale device an alternative route for studying the intrinsic properties of solid-state materials the case of semiconducting TaGeIr, Angew. Chem. Int. Ed. **59**, 11136 (2020).

[37] S. Hamann, *et al.*, Fermi-surface reconstruction at the metamagnetic high-field transition in uranium mononitride, Phys. Rev. B **104**, 155123 (2021).

[38] T. Helm, *et al.*, Field-induced compensation of magnetic exchange as the possible origin of reentrant superconductivity in UTe_2, Nat. Commun. **15**, 37 (2024).

[39] P. Rogl and P. E. Potter, The B-Pu (boron-plutonium) system, J. Phase Equilib. **18**, 467 (1997).

[40] B. J. McDonald and W. I. Stuart, The crystal structure of some plutonium borides, Acta Crystallogr. **13**, 447 (1960).

[41] A. B. Shick, L. Havela, A. I. Lichtenstein, and M. I. Katsnelson, Racah materials role of atomic multiplets in intermediate valence systems, Sci. Rep. **5**, 15429 (2015).

[42] M. Hosen, *et al.*, Observation of gapped state in rare-earth monopnictide HoSb, Sci. Rep. **10**, 12961 (2020).

[43] P. E. Blöchl, Projector augmented-wave method, Phys. Rev. B **50**, 17953 (1994).

[44] G. Kresse and D. Joubert, From ultrasoft pseudopotentials to the projector augmented-wave method, Phys. Rev. B **59**, 1758 (1999).

[45] G. Kresse and J. Hafner, *Ab initio* molecular dynamics for liquid metals, Phys. Rev. B **47**, 558 (1993).

[46] G. Kresse and J. Furthmuller, Efficient iterative schemes for *ab initio* total-energy calculations using a plane-wave basis set, Phys. Rev. B **54**, 11169 (1996).

[47] J. P. Perdew, K. Burke, and M. Ernzerhof, Generalized gradient approximation made simple, Phys. Rev. Lett. **77**, 3865 (1996).

[48] S. L. Dudarev *et al.*, Electron-energy-loss spectra and the structural stability of nickel oxide An LSDA+U study, Effect of Mott-Hubbard correlations on the electronic structure and structural stability of uranium dioxide, Phys. Rev. B **57**, 1505 (1998); Philos. Mag. B 75, 613 (1997).

[49] V. I. Anisimov, J. Zaanen, and O. K. Andersen, Band theory and Mott insulators Hubbard U instead of Stoner I, Phys. Rev. B **44**, 943 (1991).

[50] B. Dorado, *et al.*, Advances in first-principles modelling of point defects in UO_2 f electron correlations and the issue of local energy minima, J. Phys.: Condens. Matter **25**, 333201 (2013).

[51] See Supplemental Material at http://link.aps.org/supplemental/10.1103/hwpn-gll9 for Secs. I and II, which provide a more detailed description of the ground-state search and magnetic ordering in PuB_6.

[52] A. B. Shick, *et al.*, Coulomb-U and magnetic-moment collapse in δ-Pu, Europhys. Lett. **69**, 588 (2005).

[53] L. V. Pourovskii *et al.*, Dynamical mean-field theory investigation of specific heat and electronic structure of α- and δ-plutonium, Phys. Rev. B **75**, 235107 (2007).

[54] W. Ko, *et al.*, Atomic and electronic structure of an alloyed topological insulator, $Bi_{1.5}Sb_{0.5}Te_{1.7}Se_{1.3}$, Sci. Rep. **3**, 2656 (2013).

[55] M. Pickem, E. Maggio, and J. M. Tomczak, Resistivity saturation in Kondo insulators, Commun. Phys. **4**, 226 (2021).

[56] P. Syers, D. Kim, M. S. Fuhrer, and J. Paglione, Tuning bulk and surface conduction in the proposed topological kondo insulator SmB_6, Phys. Rev. Lett. **114**, 096601 (2015).

[57] X. Lei, *et al.*, Surface-induced linear magnetoresistance in the antiferromagnetic topological insulator $MnBi_2Te_4$, Phys. Rev. B **102**, 235431 (2020).

[58] Y. Shiomi and E. Saitoh, Linear magnetoresistance in a topological insulator Ru_2Sn_3, AIP Adv. **7**, 035011 (2017).

[59] J. Feng, *et al.*, Large linear magnetoresistance in Dirac semimetal Cd_3As_2 with Fermi surfaces close to the Dirac points, Phys. Rev. B **92**, 081306(R) (2015).

[60] M. Novak, *et al.*, Large linear magnetoresistance in the Dirac semimetal TlBiSSe, Phys. Rev. B **91**, 041203(R) (2015).

[61] S. K. Kushwaha, *et al.*, Bulk crystal growth and electronic characterization of the 3D Dirac semimetal Na_3Bi, APL Mater. **3**, 041504 (2015).

[62] S. Thomas, *et al.*, Weak antilocalization and linear magnetoresistance in the surface state of SmB_6, Phys. Rev. B **94**, 205114 (2016).

[63] S. Singh, *et al.*, Linear magnetoresistance and surface to bulk coupling in topological insulator thin films, J. Phys.: Condens. Matter **29**, 505601 (2017).

[64] H. Lu and L. Huang, Quasiparticle multiplets and 5f electronic correlation in prototypical plutonium borides, J Phys.: Condens. Matter **34**, 215601 (2022).

[65] J. H. Shim, K. Haule, and G. Kotliar, Fluctuating valence in a correlated solid and the anomalous properties of δ-plutonium, Nature (London) **446**, 513 (2007).

[66] M.-T. Suzuki and P. M. Oppeneer, Dynamical mean-field theory of a correlated gap formation in plutonium monochalcogenides, Phys. Rev. B **80**, 161103(R) (2009).

[67] J.-X. Zhu, *et al.*, Electronic structure and correlation effects in $PuCoIn_5$ as compared to $PuCoGa_5$, Europhys. Lett. **97**, 57001 (2012); Nat. Commun. **4**, 2644 (2013).

[68] M. Cococcioni and S. de Gironcoli, Linear response approach to the calculation of the effective interaction parameters in the LDA+U method, Phys. Rev. B **71**, 035105 (2005).

[69] See Supplemental Material at http://link.aps.org/supplemental/10.1103/hwpn-gll9 for Sects. III–V, which provide a more detailed description on the effect of Hubbard U on the lattice structure and electronic band structure, tight-binding model used, and the linear response approach to determine the Hubbard U.

[70] L. Fu, M. Kornbluth, Z. Cheng, and C. A. Marianetti, Group theoretical approach to computing phonons and their interactions, Phys. Rev. B **100**, 014303 (2019).

[71] P. A. Alekseev, *et al.*, Lattice dynamics of intermediate valence semiconductor SmB_6, Europhys. Lett. **10**, 457 (1989).

[72] M.-E. Boulanger, *et al.*, Field-dependent heat transport in the Kondo insulator SmB_6 Phonons scattered by magnetic impurities, Phys. Rev. B **97**, 245141 (2018).

[73] J. Knolle and N. R. Cooper, Excitons in topological Kondo insulators theory of thermodynamic and transport anomalies in SmB_6, Phys. Rev. Lett. **118**, 096604 (2017).

[74] M. E. Valentine, *et al.*, Breakdown of the Kondo insulating state in SmB_6 by introducing Sm vacancies, Phys. Rev. B **94**, 075102 (2016).